IEEE Access
Multidisciplinary ⋮ Rapid Review ⋮ Open Access Journal

Received 3 February 2024, accepted 14 February 2024, date of publication 21 February 2024, date of current version 1 March 2024.

*Digital Object Identifier 10.1109/ACCESS.2024.3368384*

RESEARCH ARTICLE

# Super-Resolution Level Separation: A Method for Enhancing Electroencephalogram Classification Accuracy Through Super-Resolution Level Separation

**HANG SUN, CHANGSHENG LI, AND HE ZHANG**
Department of Mechanical Engineering, Nanjing University of Science and Technology, Nanjing, Jiangsu 210094, China
Corresponding author: Changsheng Li (12012128@njust.edu.cn)

This work involved human subjects or animals in its research. The authors confirm that all human/animal subject research procedures and protocols are exempt from review board approval.

**ABSTRACT** Accurate identification of electroencephalogram (EEG) signals forms the basis for the development and application of brain–computer interface (BCI) devices. Signal preprocessing is an essential part of most EEG classification and recognition systems.In this study, we proposed a method called Super-resolution level separation (SRLS) to add dimensions of information to the classification model. First, we calculated the correlation between the EEG signals acquired by each channel and divided these channels into multiple levels. Next, we used a super-resolution method to calculate common EEGs (C-EEGs) acquired by the channels. In addition, we designed an EEG–split-informer (ES-informer) model based on an informer model to enable small-sample users to obtain highly fitting C-EEGs. We then calculated the difference between the C-EEG and true EEG (T-EEG) to obtain the unique EEGs (U-EEGs) acquired by each channel, thus, adding dimensions to the data inputted to the classification model. Utilizing the 2008 2a motor imagery (MI) EEG dataset from the BCI Competition and the P300 paradigm data collected, EEGNet was employed as the classification model to validate the efficacy of the proposed SRLS method. The results of the experiments indicated that the SRLS method augmented the input dimension of the model and amplified the classification accuracy by over 7% for MI and 3.6% for P300. These findings demonstrate that SRLS is capable of enhancing the recognition accuracy of EEG.

**INDEX TERMS** Brain–computer interface, deep learning, electroencephalogram, EEG–split-informer, super-resolution.

## I. INTRODUCTION

Berger detected the electroencephalogram (EEG) and described it as a ''window into the brain'' [1]. EEG signals can be used to analyze neural activities in the brain and study the brain from a new perspective. With the rapid development of science and technology in recent decades, extensive research has been conducted on brain activity. Many researchers have studied the brain from the perspectives of magnetoencephalography (MEG) [2] and functional magnetic resonance imaging [3]; however, EEG dominates the field. Developing a wearable, noninvasive EEG acquisition device is a promising research area. Medically, EEG signals can be used to diagnose epilepsy [4], alert patients before seizures occur, and analyze neurologic manifestations in severe COVID-19 cases [5]. In addition, EEG-based analysis can aid in cross-subject emotion recognition [6]. However, researchers are not satisfied with passive EEG analysis and are actively seeking ways to control external devices directly by the brain. Brain–computer interface

The associate editor coordinating the review of this manuscript and approving it for publication was Humaira Nisar.

(BCI) has emerged as a communication system that bypasses the brain's normal output pathways of peripheral nerves and muscles [7] to enable the brain to directly control external devices.

The first step in establishing a BCI is the selection of a control scheme. Steady-state visual evoked potentials (SSVEPs) have been used in many applications. Na et al. designed an embedded, lightweight SSVEP-BCI electric wheelchair [8], and Liu et al. designed a SLAM-SSVEP system to enable users to control a vehicle equipped with lidar by using their minds [9]. Another method is motor imagery (MI), in which users imagine limb motions to input data into the BCI. Thenmozhi et al. improved the classification performance of MI signals for BCI [10]. Attallah et al. used MI-BCI to assist people with limb motor disabilities by enabling them to control assistive devices through their brain signals [11]. AK et al. used GoogLeNet to test whether subjects can control a robot manipulator by using MI [12]. Event-related potentials (ERPs) are also key to BCI applications. Zhang et al. developed a novel 36-class bimodal ERP-BCI system based on tactile and auditory stimuli [13], and Wu et al. studied the effect of noise on ERP-BCI in a real environment to establish a generalized method for BCI [14]. Researchers have combined multiple control schemes to establish a hybrid BCI. For example, Choi et al. combined eye-blink with MI to allow users to complete a gait task by wearing a lower-limb exoskeleton through the developed real-time BCI controller [15]. However, for any BCI control scheme, the key point is how to enhance the accuracy of the acquired EEG signal. In most cases, this accuracy can be intuitively understood as the EEG classification accuracy. The examination of EEG signals is frequently compared to the cocktail party problem, which involves analyzing indeterminate information in the brain through restricted channels. For example, techniques like independent component analysis and principal component analysis are utilized to process EEG signals. This aids in isolating the characteristics of subjects at a specific moment. Inspired by the concept of feature extraction, we proposed an EEG Super-resolution level separation (SRLS) model to separate a single EEG acquisition channel into information that is common to other channels and information independent of other channels. Super-resolution (SR) can be considered a method of signal amplification, designed to acquire more comprehensive information from limited input data. Li et al. [2] designed Wasserstein generative adversarial networks (WGANs) to obtain virtual acquisition channels by using the existing EEG channel and improve the classification accuracy. Corley and Huang [16] upsampled the EEG channel by using generative adversarial networks (GANs). By using the deep CNN-based SR method, Kwon et al. demonstrated that various brain dynamics can be explored using a small number of sensors [17]. The SR method reduces the number of EEG channels required when using the BCI and yields a good result. The common information among different EEG acquisition channels is used to deduce the EEG signal in the target channel; however, the independent information of a single channel cannot be supplemented. As such, we proposed an SRLS method. In this method, first, the correlation between the EEG acquisition channels is calculated. Next, the channels are divided into multiple levels. At each level, the SR method is used to deduce the EEG signal on the target channel as the common information. The difference between the channels is treated as independent information. Existing SR methods require long-time data and large sample capacity to obtain a good SR result. For instance, in a study [18], 5144 h of data were used. In the current study, an EEG-Split-informer (ES-informer) model transformed from an informer model suitable for time-series forecasting was used to perform Super-resolution calculations by using approximately 27 min of data and 288 samples or use a 10-minute P300 dataset, and the common and independent information of each EEG channel at different levels were obtained. Next, the two types of information were inputted into the classification model. In conclusion, the EEGNet model was utilized to confirm that the SRLS method is capable of enhancing the input dimension of data and augmenting the classification accuracy of EEG in both MI and P300 paradigms.

## II. RELATED WORKS AND MOTIVATION

### A. PURPOSE OF EEG ANALYSIS

The primary objective of an EEG-based BCI system is to analyze the EEG signals of subjects and to enhance the precision and range of applications of the system. In contrast to sound or text, EEG is similar to an abstract notion that is typically challenging to articulate in an intuitive manner. Therefore, many classification methods have been proposed. Many mainstream classification methods are based on deep learning (DL). Classification based on convolutional neural networks (CNNs) and recurrent neural networks (RNNs) can yield a considerably high accuracy [19], [20]. With the development of DL, numerous novel and combined classification networks have been proposed to improve EEG classification accuracy. For example, Khademi et al. proposed an MI classification method based on CNN and long short-term memory (LSTM) to improve the classification accuracy considerably [21]. Li et al. developed a simplified Bayesian convolutional neural network (SBCNN) to enable users to complete a game task through the online P300 BCI [22]. Willett et al. aided users with disabilities in completing imagery writing [23]. Among the classification models, EEGNet proposed by Lawhern et al. has received increased attention from researchers because of its lightweight and high classification performance [24] and has been transformed into a classification model for use in different tasks. For instance, Deng et al. designed a TSGL-EEGNet [25] for MI classification.

In addition to modifying the model structure, EEG processing or feature extraction improves the classification accuracy of the BCI system because it can highlight the EEG features of subjects with different behaviors. Although Craik et al. found that processing EEG into images does not improve

the classification accuracy in some cases, this goes against the intuition that the more effort applied to the preprocessing stages, the more accurate the classification will be [26]. Nevertheless, many classification models require feature extraction. For instance, the common spatial pattern (CSP) is an effective feature extraction method for EEG classification [27] and can effectively distinguish MI to adapt to the BCI device [28]. Independent component analysis (ICA) is effective in separating the signal into independent components (ICs) to enhance classification accuracy [29]. Continuous wavelet transform (CWT) can be used to analyze EEG signals from the perspective of the time–frequency domain to improve the MI classification accuracy [30].

In this research, to increase the recognizable information dimension of EEG, the SRLS method was applied to process the EEG signals derived from MI and P300. Subsequently, EEGNet was utilized to examine the influence of SRLS on classification accuracy. The datasets employed in this study are characterized as follows.

### B. DATASET 1

The BCI Competition IV dataset 2a public EEG dataset [31] was used to verify the effectiveness of the SRLS method proposed in this paper. This dataset contains recordings of 4-class MI tasks (left hand, right hand, feet, and tongue) performed by nine healthy subjects by using 22 noninvasive EEG acquisition channels at 250 Hz (Fig. 1). Each subject participated in two sessions, and each session comprised approximately 27 min of data, with 288 recorded data samples per session and 72 samples per class. The duration of each motion class was recorded as one cycle. The time when the subject heard a prompt tone was recorded as the starting time t = 0. The motion to be executed by the subject was displayed on the screen in the form of an arrow at t = 2-3.25 s and was then changed to a "+" to guide the subject's point of view and weaken the influence of the electro-oculogram (EOG) signal. The subject performed the designated MI task from t = 3-6 s until the "+" disappeared from the screen, completing one cycle of recorded motion. The recording flow is shown in Fig. 2.

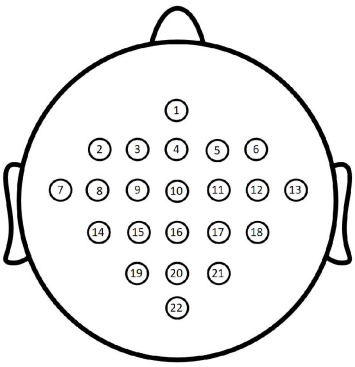


**FIGURE 1.** Distribution of the acquisition channels.

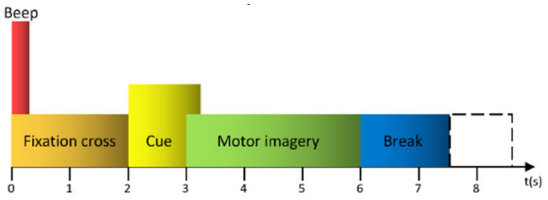


**FIGURE 2.** The timing of a sample collection, including MI prompt, execution, rest process.

According to the MI collection methodology, both the training and testing sets comprised 288 samples each. The training was concentrated on four types of MI to assess the applicability of SRLS. In this study, this dataset was the primary focus for in-depth analysis and comprehensive comparison to ascertain the effectiveness of SRLS.

### C. DATASET 2

Dataset 2 was based on the P300 paradigm. Six subjects participated in this experiment; all were previously informed about the experiment's purpose and method and consented to partake in it. The subjects focused on the screen as depicted in Fig. 3a), and the six items displayed would randomly flicker, as shown in Fig. 3b). The subjects concentrated on the object on the screen as prompted. When the object flickered, a P300 signal was produced in the subjects, distinctly different from EEG signals without the P300 component. The study employed an electrode cap to gather EEG data from the 10 channels illustrated in Fig. 4, with a sampling frequency of 1,000 Hz. For each subject, each flicker was recorded as a sample, with each experiment yielding 900 to 1,000 samples. Half of these samples were selected for the training set, and the remainder formed the testing set. This dataset functioned as a validation set to broaden the scope of SRLS's applicability and was not subjected to detailed analysis.

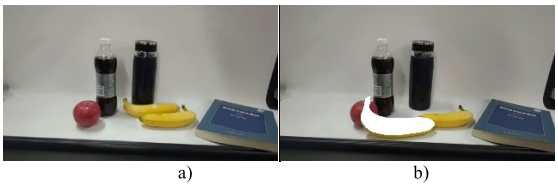


**FIGURE 3.** a) User gaze image and b) is target flicker.

### D. DATA PROCESSING

The EEG signal is nonstable, susceptible to external interference, and sensitive to global baseline drift; this can hinder signal processing and identification. Therefore, the EEG signal was processed using common average referencing (CAR). First, the average value of the EEG signals acquired from all acquisition channels was calculated. Next, the difference between the average and the original EEG signal values was computed using (1), where $x_i^{CAR}$ is the calculated value of the

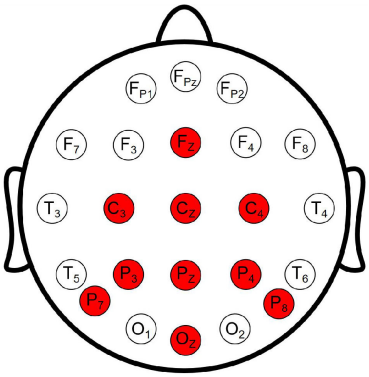


**FIGURE 4.** EEG channels used in the P300 experiment.

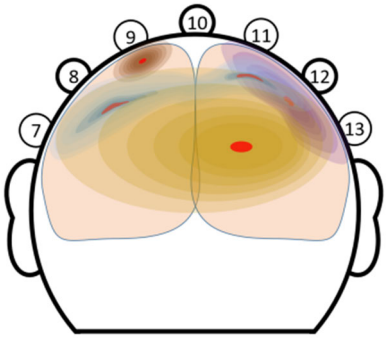


**FIGURE 5.** EEG generated in different parts of the brain is superimposed, affecting the final resolution.

EEG signal acquired by channel i, $x_i(t)$ is the original value of the EEG signal acquired by channel i, and C is the total number of channels used (C = 22 in this study). The EEG processed using CAR had less internal and external noise and retained the EEG signal.

$$x_i^{CAR} = x_i(t) - \frac{1}{C}\sum_{j=1}^{C} x_j(t) \tag{1}$$

According to the Nyquist sampling theorem, the device used in the experiment was able to acquire EEG signals below 125 Hz. However, not all channel signals needed to be analyzed. Previous studies on EEG have shown that the EEG signal ranges produced by MI are mainly in the $\mu$ and $\beta$ bands (i.e., 8–30 Hz) [32], [33]. Prior to final processing, a fifth-order zero-phase Butterworth filter was used for bandpass filtering of the EEG signals processed by CAR at 8–30 Hz to retain the information within this frequency band. The data were then processed using the SRLS method. EEG signals within 8–30 Hz were retained in the final classification to highlight the effective signals and reduce overfitting.

### E. SRLS METHOD

The EEG signals acquired by each channel of the noninvasive EEG device are the superposed data of each neuron and other neurons in the cranium after reflection and refraction. Even after CAR, each acquisition channel contains the information of other channels. The independent information specific to each channel cannot be separated further.

Fig. 5 depicts a cross-sectional diagram of the process for acquiring EEGs (for reference only). When a person thinks, specific neurons change their potentials (the red part in Fig. 5) and produce potential differences that may drive the change in the potentials of surrounding neurons until being acquired by some EEG channels. When the potential change is strong, many channels get affected, and related channels contain common information (C-EEG), burying the unique EEG (U-EEG) generated by superficial neurons and weak potential changes in the brain. Consequently, the U-EEGs cannot be effectively utilized. The proposed SRLS method separates the U-EEG and C-EEG around each channel, highlighting the distinctive features of the EEGs and increasing the input data volume of the classification model. As a result, the accuracy of EEG identification and classification can be enhanced. The proposed SRLS method comprises two steps: 1) calculating the correlation coefficient and correlation between the channels and dividing the channels into several levels, and 2) using an ES-informer to compute the U-EEGs and C-EEGs acquired by the EEG channels at each level and separating the predicted EEG ($EEG_P$) and difference EEG ($EEG_D$) from the original EEG ($EEG_T$).

The number of C-EEGs among the channels can be determined based on the correlation between the channels. The correlation coefficient $\rho_{ij}$ between two channels can be calculated using the covariance (2). In (2), $i$ and $j$ represent two channels, L is the data length of the sample, and $\bar{P}_i$ and $\bar{P}_j$ represent the average values of the two channels. The calculated correlation coefficient $\rho_{ij}$ has positive and negative values: a positive value indicates that the two channels are positively correlated, whereas a negative value indicates that the two channels are negatively correlated. In this study, the absolute value of the correlation coefficient $\rho_{ij}$ was used. When $\rho_{ij}$ approaches 1, it indicates that many C-EEGs are contained in the EEGs acquired by the two channels; in contrast, when $\rho_{ij}$ approaches 0, it implies that many U-EEGs are contained in the EEGs acquired by the two channels.

$$\rho_{ij} = \left| \frac{\sum_{l=1}^{L} (P_{il} - \bar{P}_i)(P_{jl} - \bar{P}_j)}{\sqrt{\sum_{l=1}^{L} (P_{il} - \bar{P}_i)^2 \times \sum_{l=1}^{L} (P_{jl} - \bar{P}_j)^2}} \right| \tag{2}$$

$$\overline{\rho}_{ij} = \frac{1}{9}\sum_{S=1}^{9} \rho_{sij} \tag{3}$$

By using (2) and (3), the average correlation coefficients among the 22 channels for nine subjects in the dataset were calculated and plotted into a two-dimensional (2D) Fig. 6 to observe the number of C-EEGs among the channels intuitively.

Taking the left channel EEG-8 (C3) as an example, its $\rho_{ij}$s with other channels were obtained and ranked in descending order as follows: EEG-7, EEG-14, EEG-2, EEG-17, EEG-18, EEG-9, EEG-12, EEG-11, EEG-13, EEG-21, EEG-3, EEG-15, EEG-6, EEG-20, EEG-22, EEG-5, EEG-16, EEG-4, EEG-1, EEG-19, and EEG-10. In this research,

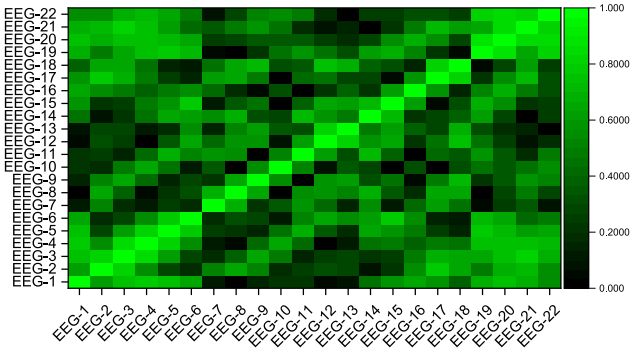


**FIGURE 6.** For EEG correlation among different acquisition channels, 1.0 is completely correlated and 0.0 is completely uncorrelated.

during the execution of the SRLS process on MI, a balance was struck between the number of channels collected by the EEG and the input tensor requisites of the model. This balancing act was essential to determine the quantity of layers in the model and the number of channels included within each layer. In the study, the top 16 channels were selected and divided into four levels: *L0*, *L1*, *L2*, and *L3*. Each level contains four channels. To differentiate between EEG signals processed at varying levels, the signal resulting from the combination of channels exhibiting a strong correlation was termed a superficial layer, denoted by a lower numerical value (for instance, *L0*). Conversely, the signal characterized by opposite features was referred to as a deep layer and was assigned a larger layer number (such as *L3*). The division method is illustrated in Fig. 7 a). In the SRLS, the channels at each level were trained using the same ES-informer to obtain the C-EEGs contained in each channel. We did not probe *L4*, which contains five channels and requires an independent ES-informer different from the former four levels. Also, because these five channels have a low correlation with the target channel, the signals separated out are not significant. As can be seen in Fig. 7 a), the $\rho_{ij}$s of some right channels with channel EEG-8 (C3) were closer to 1 than those of the left channels, reflecting the existence of event-related synchronization (ERS) and event-related desynchronization (ERD). The level division of the right channels correlated with EEG-12 (C4) was plotted in the same manner (Fig. 7 b)). As observed by comparison,

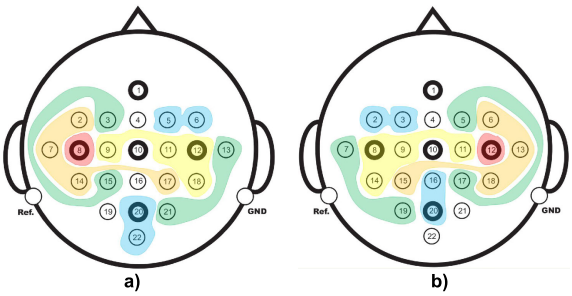


**FIGURE 7.** a) is distribution of $\rho_{ij}$ between EEG-8 and other channels b)is distribution of $\rho_{ij}$ between EEG-12 and other channels.

the level divisions of the two parts of channels are generally symmetric, comply with the physiological structure features of the human brain, and thus can support the SRLS method.

These results prove that there were obvious or unobvious correlations between the EEGs acquired by the channels. There was some superposed information among the channels. For instance, the EEGs acquired by channel EEG-8 contained some information contained in EEG-2, EEG-17, and other EEG channels. However, the superposed information cannot be separated using traditional methods such as CAR and recursion. The ES-informer is suitable for calculating the EEG information in the target channel based on several input channels. In the ES-informer, the C-EEGs of the input channels and the target channel can be integrated, forming $EEG_{Pl}$, where $l$ is the level number representing *L0*, *L1*, *L2*, and *L3*. The U-EEG of the target channel is difficult to reproduce but can be calculated using the difference between $EEG_T$ and $EEG_{Pl}$ and recorded as $EEG_{Dl}$. That is, the equation satisfying (4). In this manner, the superficial and deep EEG data can be separated.

$$EEG_{Dl} = EEG_T - EEG_{Pl} \tag{4}$$

Considering that most existing SR methods require a long acquisition time and a large dataset, we designed an EEG-Split-informer (ES-informer) model suitable for short-time and small datasets to supplement the information of the target channel. This ES-informer model is a variant of the informer [34] model and originated from the transformer model with a multilayer encoder and decoder commonly used in image identification and behavior identification. To make the transformer model more adaptable to time-series forecasting, the creator of the informer model introduced the concept of timestamps that considered the influence of hour, day, week, and holiday on the studied signal. Thus, the informer model was created. In the informer model, the volume of trained data can be increased by sliding the window to avoid the need for large sample capacity and high computer hardware configuration. Moreover, a self-attention distilling operation was proposed to reduce the number of parameters required by the model, effectively lowering the application threshold of the informer so that PC users can use the informer to perform time-series forecasting tasks. Although the EEG signals may be affected by the subjects' ages, BCI service time, and other macroscopic factors, their specific signals vary from person to person and exhibit high randomness and burstiness. Therefore, for a short-time dataset, the demand for different time stamps is not significant. To perform SR processing of EEG signals by using the informer, the original informer model was modified to create an ES-informer model.

The input channel of the ES-informer model comprises n channels $C_i \in \{C_1, .., C_n$ ($n \leq 21$; $n = 4$ in this study). Different levels of output SR channels $C'_{pl}$ were compared with the target channel $C_p$ serving as the tag value, where $C_p \notin C_1, .., C_n$ ($l$ is the level number, and $EEG_{Pi}$ is the information in $C'_{pl}$). In addition, the input data were

disordered during the training of the informer to prevent treating the sequence of the time series as the time information in a single sample. To calibrate the time information of the data, sinusoidal position encoding methods such as the pointwise self-attention mechanism and the time stamps were used in the model, as expressed in (5).

$$\begin{cases} PE_{(pos,2j} = \sin\left(\dfrac{pos}{(2L_x)^{\frac{2j}{d_{model}}}}\right) \\ PE_{pos,2j} = \sin\left(\dfrac{pos}{(2L_x)^{\frac{2j}{d_{model}}}}\right) \end{cases} \tag{5}$$

In (5), the encoded time value PE at a specific time depends on the oddity of a signal position, pos (the index position of data in the time series) on the time series at this time and is encoded sinusoidally within the range of 0–1. The value of pos can range throughout the time series and can be the index of partial time. $L_x$ is the length of the time series, $d_{model}$ is the dimensionality of the input and output vectors of the model, and $j \in \{1, 2, \ldots, [d_{model}/2]\}$. The content in the bracket distinguishes the positions and cycles of a data point. This encoding method can prevent vanishing or exploding gradient problems and reduce overfitting and noise. In the ES-informer model, the pos is related only to an instantaneous moment and is irrelevant to the position of a sample in all the samples. Therefore, the timestamps of the input information were set as partial time indices, and their relative position information $pos_i$ belonged to $\{0, 1, 2, \ldots, L-1\}$. The $pos_i'$ of the target Super-resolution channel was equal to $\{t_s, t_s+1, t_s+L'-1\}$, where $t_s$ is the initial code of the output tag and $L'$ is the length of the output time series and satisfies the following condition (6):

$$\begin{cases} t_s \geq 0 \\ t_s + L' - 1 \leq L - 1 \end{cases} \tag{6}$$

The EEG obtained by the ES-informer model through the super sampling channel $C_{pl}'$ is not a predicted data, and its timestamps are included in the timestamps of the input data. This method considers the effect of the pre-order information on the post-order information, weakens the influence of path and time on the EEG propagation in the cranium, and increases the amount of common information in the super sampling channel $C_{pl}'$.

For a sample at time $t$, the input data was $X^t = \{x_1^t, \ldots, x_{L_x}^t | x_i^t \in \mathbb{R}^{d_x}$, where $d_x$ is the number n of EEG signal input channels (n = 4). The data outputted by the ES-informer model satisfied $\mathcal{Y}^t = \{y_1^t, \ldots, y_{L_x}^t | y_i^t \in \mathbb{R}^{d_y}\}$, where $d_y$ is the output channel $C_{pl}'$, $\mathcal{Y}^t$ is the EEG information value of channel $d_y$ at time t. The relationship between the input channel and the SR channel is shown in Fig. 8.

Similar to the informer, the ES-informer model contains a two-layer encoder and a one-layer decoder, with a structure as shown in Fig. 9.

The three tensors, namely Query ($Q$), Key ($K$), and Value ($V$), shown in the multihead probSparse self-attention

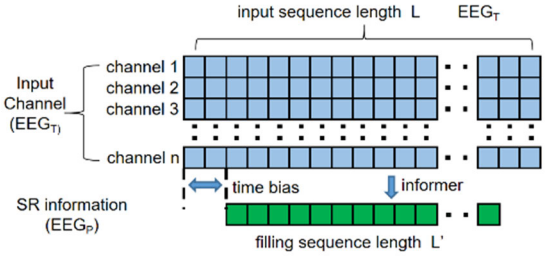


**FIGURE 8.** The $EEG_P$ is obtained using the $EEG_T$ of multiple channels.

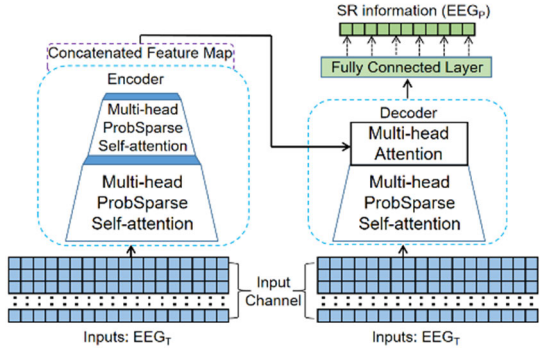


**FIGURE 9.** Schematic diagram of the ES-informant structure.

block in Fig. 9, were calculated using three linear layers, $Q \in R^{L_Q \times d}$, $K \in R^{L_k \times d}$, and $V \in R^{V_Q \times d}$, respectively, where d is the dimensionality of self-attention. The self-attention in the informer was determined using (7). The probability of useful information in $\mathcal{X}^t$ showed that the ES-informer model effectively enhanced the parameter use efficiency and reduced the service demand for hardware.

$$\mathcal{A}(q_i, K, V) = \sum_j^{L_V} \frac{k(q_i, k_j)V_j}{\sum_l^{L_K} k(q_i, k_l)} \tag{7}$$

where $p(k_j|q_i) = k(q_i, k_j)/\sum_l^{L_K} k(q_i, k_l)$, and the asymmetric exponential kernel $q_i k_j^T/\sqrt{d}$ was used for $k(q_i, k_j)$. Because the self-attention probabilities are not identical, only partial $Q$s and $K$s are significantly correlated. If attention is paid to some important $Q$s, the remaining $Q$s are substituted with their hypodispersion; this reduces the complexity of the model. The importance of $Q$ was measured using Kullback–Leibler divergence (8).

$$KL(q \parallel p) = ln \sum_{l=1}^{L_K} exp\left(\frac{q_i k_l^T}{\sqrt{d}}\right) - \frac{1}{L_k}\sum_{l=1}^{L_K} \frac{q_i k_i^T}{\sqrt{d}} - lnL_k \tag{8}$$

Finally, a softmax function was used to obtain the most important Q (9):

$$\mathcal{A}(\overline{Q}, K, V) = softmax(\frac{\overline{Q}K_T}{\sqrt{2}})V \tag{9}$$

Although the above method obtains important information in $\mathcal{X}^t$ and reduces the complexity of the model, the length of the time series outputted by each layer of the encoder

remains unchanged. With the superposition of encoder layers, memory usage increases significantly, which is not conducive to the massive calculation of data. To address this issue, the self-attention distilling operation is conducted between two encoder layers. In this operation, the maximum-pooling layer is used to exclude minor features and focus on major features. This operation reduces the memory usage (10).

$$X_{j+1} = MaxPool(ELU(Conv1d([X_j]_{AB}))) \tag{10}$$

where $[\cdot]_{AB}$ includes the key operations of multihead ProbSparse self-attention and attention block, Conv1d(·) is the 1D convolution on the time series, ELU(·) is the activation function, and MaxPool(·) is the maximum-pooling layer with a step length of 2. With the increase in the number of encoder layers after the self-attention distilling operation, the cumulative time-series length at each layer was half of that in the upper layer; this restricted the data volume of the model parameters and reduced the demand for video memory of the GPU.

In the application of the ES-informer for signal processing, the division of training and testing sets adhered to the guidelines established in the BCI Competition IV dataset 2a experiment. The parameters utilized during the training phase are presented in Table 1.

**TABLE 1. Parameters used by ES-informer.**

| Argument | Value | Argument | Value |
|---|---|---|---|
| train epochs | 15 | batch_size | 64 |
| seq len | 36 | label_len | 6 |
| learning_rate | 0.0005 | $d_{model}$ | 128 |
| optimizer | Adam | Loss- function | MSELoss |

The ES-informer model was used to acquire the EEG information included in each SR channel $C'_{pl}$ of the channels $C_p$ at different levels. Based on (2), the correlation $\rho_{ij}$ between the $EEG_{Pl}$s at *L0*, *L1*, *L2*, and *L3* was plotted as shown in Fig. 10.

$EEG_{Pl}$ is the C-EEG at the aforementioned LC, and $EEG_{Dl}$ is the U-EEG at LC, where $LC \in \{L0, L1, L2, L3\}$, $C$ is the level of the currently obtained EEG. As can be seen in Fig. 10, the $\rho_{ij}$ between the SR channels $C'_{pl}$ in the superficial layer was slightly higher than that between $C_p$s, whereas that in the deep layer was lower than that between $C_p$s. To intuitively prove this result, channels with identical rank orders were superposed and the average value was determined. Next, the $\rho_{ij}$ between the channels at different *LC*s was plotted again. Furthermore, the $\rho_{ij}$ between U-EEGs of the channels at each *LC*s was calculated in the same manner, as demonstrated in Fig. 11.

As can be seen in Fig. 11, the $\rho_{ij}$ between the channels with $EEG_{Pl}$ obtained at the superficial layer LC was strong, whereas that between the corresponding $EEG_{Dl}$s of the channels was weak. To show the variation in the waveforms of $EEG_T$, $EEG_{Pl}$, and $EEG_{Dl}$ at different levels, the channel EEG-8 of subject 4 was taken as an example to plot the waveforms of $EEG_T$, $EEG_{P0}$, $EEG_{D0}$, $EEG_{P3}$, and $EEG_{D3}$ (Fig. 12).

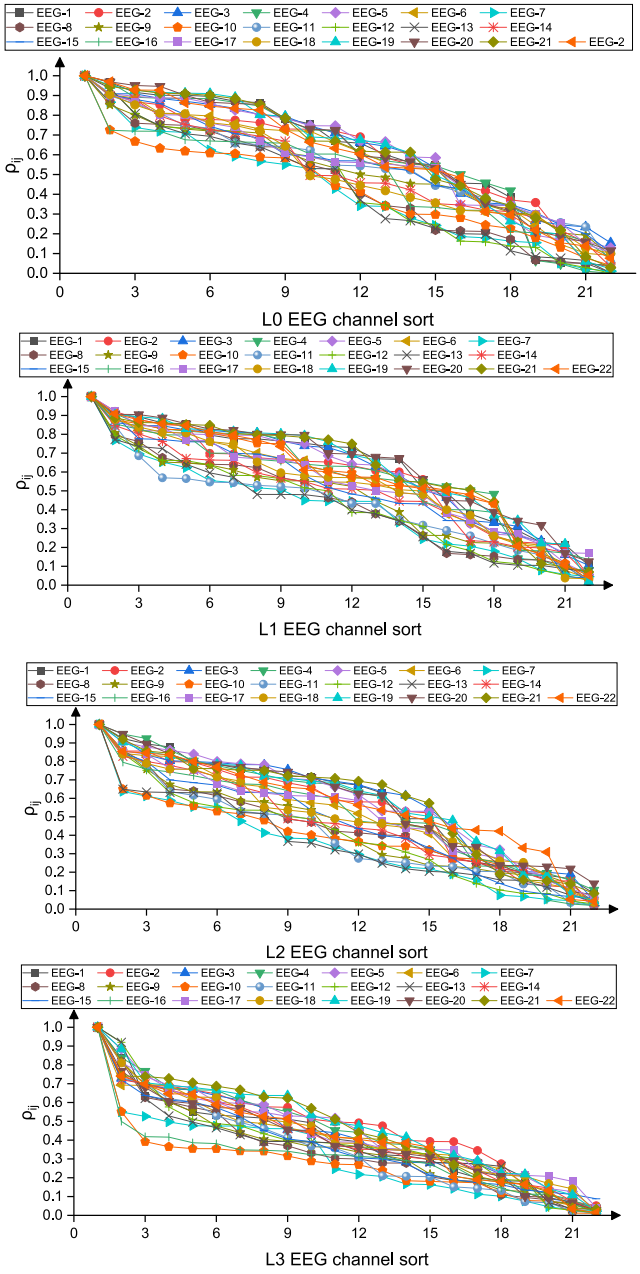


**FIGURE 10.** The $\rho_{ij}$ of the channels at *L0*, *L1*, *L2*, *L3* levels in descending order.

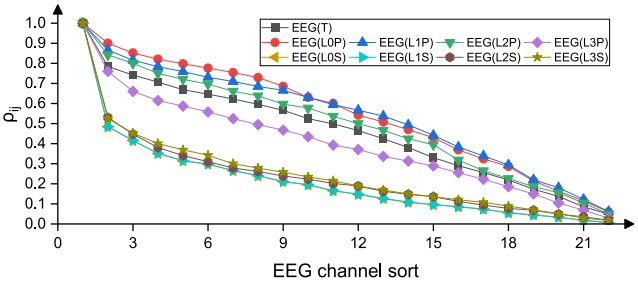


**FIGURE 11.** Average $\rho_{ij}$ in descending order.

As can be seen in Fig. 12, the $EEG_{P0}$ and $EEG_T$ at L0 were similar, the $EEG_{D0}$ at L0 tended to be stable, and that at deep level LC was the opposite, further proving that the number of

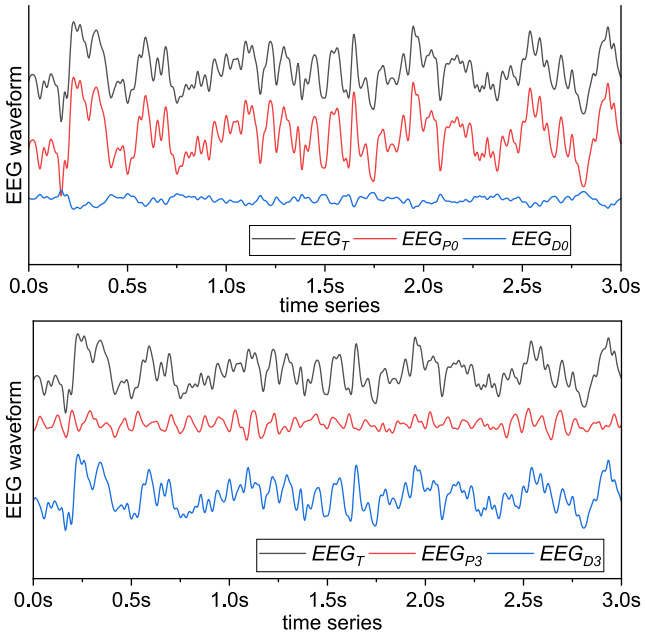


**FIGURE 12.** The calculation principle of $EEG_{DI}$.

C-EEGs among the $C_p s$ at the superficial layer is inversely proportional to the number of U-EEGs. A single BCI acquisition channel affected by the change in the potentials of superficial neurons or weak neurons contains many U-EEGs, whereas multiple acquisition *channels with EEGs affected by the change in the potentials* of deep neurons or strong neurons contain many C-EEGs. By using the ES-informer and other SR methods, EEG signals at different LCs were separated, resulting in a multifold increase in the number of input signals that can be used in the classification model. Each level of EEG is called SRLS-EEG, which can be divided into 9 kinds of input signals: $EEG_T$, $EEG_{P0}$, $EEG_{D0}$, $EEG_{P1}$, $EEG_{D1}$, $EEG_{P2}$, $EEG_{D2}$, $EEG_{P3}$, and $EEG_{D3}$.

### F. VERIFYING THE EFFECTIVENESS OF THE SRLS METHOD

To substantiate the hypothesis that SRLS enhances EEG classification accuracy, the efficacy of SRLS was evaluated through comparison using EEGNet. Various levels of $EEG_T$, $EEG_{Pl}$, and $EEG_{Dl}$ were combined to create SRLS-EEG, which was then input into EEGNet. This process enabled the acquisition of four-class results for MI and binary classification outcomes for P300, thereby facilitating an analysis of the impact of SRLS on classification results.

The EEGNet model is a compact convolutional neural network for EEG-based BCIs and has exhibited high performance in many EEG-related fields. By using DepthwiseConv2D and SeparableConv2D, the EEGNet model classifies EEG signals with an approximate logic of a common spatial pattern (CSP). On this basis, many researchers developed EEG classification models, such as the TSGL-EEGNet [25], EEG-TCNet [35]. In this study, $EEG_T$, $EEG_{Pl}$, and $EEG_{Dl}$ were inputted into the most basic EEGNet model according to the specific or total number of channels used. Except for the different number of input channels used in training the models, all the hyperparameters, as well as the quantity and size of convolution kernels, were the same in all the models. Thus, the four classification results of the types of data obtained could be compared to study the effect of EEG level separation.

To verify the effect of the proposed SRLS method on the classification results, the EEGNet classification methods was used. To alleviate unnecessary effects of the classification models with different structures on the classification accuracy, the models were set with the same hyperparameters as well as the same quantity and size of convolution kernels but different numbers of input channels depending on the EEG combination. The input combination methods in EEGNet classification methods are shown in Fig. 13. All channels were selected. Only the single-level data, such as $EEG_T$ or $EEG_{Pl}$, did not require a change in the number of channels. If different levels of data were combined, such as $EEG_{P1} + EEG_{D1}$, the samples in the EEGNet model were spliced in 2nd dimensions. The channel multiples for the input of EEGNet were calculated as the product of the actual input channels, which were 22 and 10 in this study, and the number of levels. Finally, the combined sample data were inputted into the classification model to obtain the classification accuracies in different combinations.

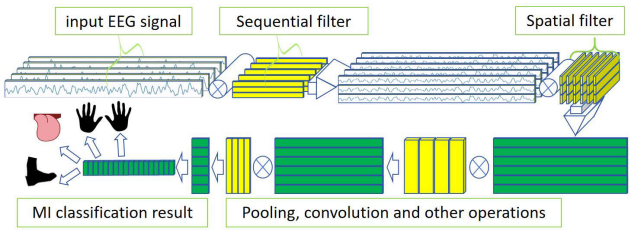


**FIGURE 13.** EEGNet model schematic (four categories of MI).

## III. RESULT

SRLS-EEG, as a method for EEG processing, is designed to broaden the analytical approaches for EEG and more effectively analyze brain activity in subjects. To clarify the influence of the SRLS method on EEG signals, EEGNet were employed as the classification model in this study. The original EEG, i.e., $EEG_T$, was used as a reference for classification results, marked as 100%, and subsequently compared with the accuracies achieved by other methods according to (11).

$$\alpha = \frac{acc_S}{acc_T} \times 100\% \tag{11}$$

where $acc_S$ is the classification accuracy achieved using EEG at different levels as input for EEGNet in SRLS-EEG; $acc_T$ is the accuracy from $EEG_T$; and $\alpha$ signifies a comparison of classification outcomes, i.e., the relative accuracy. To differentiate between models, the classification network utilizing SRLS-EEG is henceforth referred to as

SRLS-EEGNet, while the model with an input of $EEG_T$ was still called EEGNet. First, $EEG_T$, $EEG_{Pl}$, and $EEG_{Dl}$ were employed as input data to analyze the information in EEG at various levels, with the classification results depicted in Fig. 14.

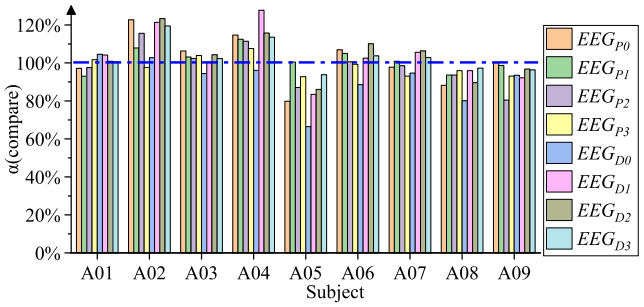


**FIGURE 14.** Direct comparison of $EEG_T$, $EEG_{Pl}$, and $EEG_{Dl}$.

In Fig. 14, the blue horizontal line represents the benchmark for $EEG_T$, indicating the scenario where the original classification accuracy is mapped to 100%. Statistical results indicated that SRLS-EEG significantly impacted classification outcomes. For most subjects, using a single-level SRLS-EEG appeared detrimental to accurate MI identification, possibly due to the dispersion of principal EEG information, making effective data extraction challenging from a single-level SRLS-EEG. In contrast, for a minority of participants, recognition accuracy notably improved, likely owing to the distinct separation of signals in the corresponding MI actions. $EEG_{Pl}$ and $EEG_{Dl}$ at the same level were integrated as input to form $EEG_{PDl}$. In other words, the original 22 input channels were reconfigured to 44 channels and introduced into EEGNet. These statistical results are presented in Fig. 15.

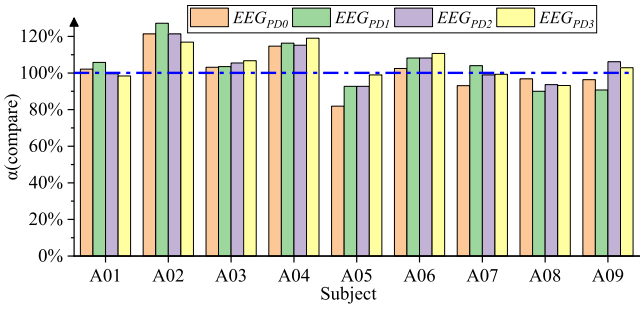


**FIGURE 15.** Direct comparison of $EEG_{PDl}$.

The statistical findings revealed that for most subjects, the classification accuracy of SRLS-EEGNet matched or exceeded that of EEGNet. Additionally, compared to using a single channel, this configuration had a more balanced effect on classification performance. However, for a minority of subjects, the influence of SRLS-EEG remained negative. Therefore, $EEG_{PDl}$ and $EEG_T$ were merged again to form $EEG_{TPDl}$, further diversifying the model's input types. The statistical outcomes obtained with this configuration are summarized in Fig. 16.

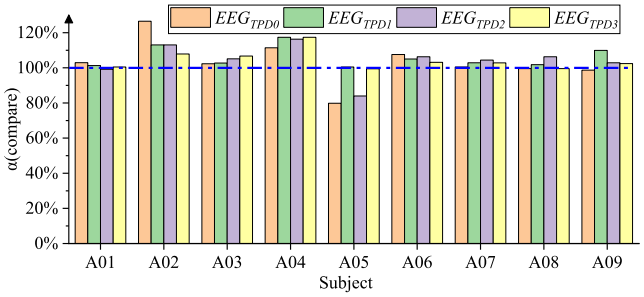


**FIGURE 16.** Comparison of $EEG_{TPDl}$ by levels.

The SRLS-EEG combination of $EEG_{TPDl}$ demonstrated greater stability, and for the majority of subjects, an enhancement in recognition accuracy was observed. Nonetheless, for some subjects or at certain levels, the recognition accuracy using SRLS-EEG as the input was still lower compared to standard EEG. Consequently, different levels of $EEG_{Pl}$ and $EEG_{Dl}$ were further combined to form $EEG_{Pall}$ and $EEG_{Dall}$. On this basis, $EEG_T$ was also added to generate $EEG_{TPall}$ and $EEG_{TDall}$. Finally, all SRLS-EEG signals were combined with $EEG_T$ to form a comprehensive input of 9 levels and 198 channels $EEG_{TPDall}$, which were then introduced into EEGNet, yielding the results shown in Fig. 17.

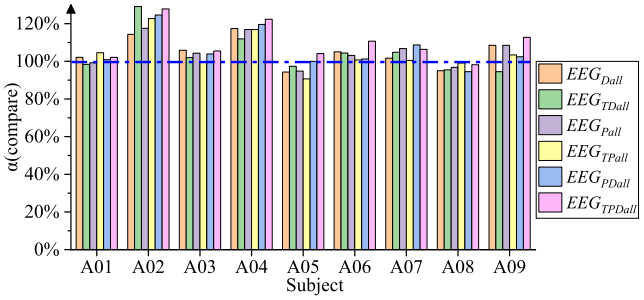


**FIGURE 17.** Comparison of $EEG_{Pall}$, $EEG_{Dall}$, and other classification types.

The aforementioned statistics demonstrated that the SRLS approach improved EEG classification accuracy for most subjects. Although the specific combination and efficacy varied individually, the overall accuracy exceeded that of EEG signals unprocessed by SRLS, validating the effectiveness of SRLS. To compare the impact of different SRLS-EEG combinations on classification accuracy, the average relative accuracy differences obtained by all subjects in different combinations are compiled into Table 2.

Subsequently, SRLS-EEG was compared with the original EEGNet, EEG-TCNet, and Shallow ConvNet [36] classification models, with the comparative results displayed in Table 3.

SRLS-EEGNet, utilizing EEGNet as the base classification model, exhibited higher accuracy than EEGNet,

**TABLE 2. Performance comparison of different levels of SRLS-EEG.**

| Combination | α | Combination | α |
|---|---|---|---|
| $EEG_{P0}$ | 1.52% | $EEG_{D0}$ | -8.76% |
| $EEG_{P1}$ | 1.70% | $EEG_{D1}$ | 3.69% |
| $EEG_{P2}$ | -1.42% | $EEG_{D2}$ | 3.68% |
| $EEG_{P3}$ | -1.67% | $EEG_{D3}$ | 3.31% |
| $EEG_{PD0}$ | 1.33% | $EEG_{TPD0}$ | -0.36% |
| $EEG_{PD1}$ | 4.28% | $EEG_{TPD1}$ | -2.27% |
| $EEG_{PD2}$ | 4.60% | $EEG_{TPD2}$ | 0.57% |
| $EEG_{PD3}$ | 5.12% | $EEG_{TPD3}$ | 0.88% |
| $EEG_{Pall}$ | 4.92% | $EEG_{Dall}$ | 4.21% |
| $EEG_{TPall}$ | 5.33% | $EEG_{TDall}$ | 4.22% |
| $EEG_{PDall}$ | 6.20% | $EEG_{TPDall}$ | 9.97% |

**TABLE 3. Comparison of MI recognition results from different classification models.**

| | EEGNet | EEG-TCNet | Shallow ConvNet | SRLS-EEGNet |
|---|---|---|---|---|
| Subject 1 | 84.34% | 85.77% | 79.51% | **89.24%** |
| Subject 2 | 54.06% | 65.02% | 56.25% | **69.79%** |
| Subject 3 | 87.54% | **94.51%** | 88.90% | 93.4% |
| Subject 4 | 63.59% | 64.91% | **80.90%** | 77.78% |
| Subject 5 | 67.39% | **75.36%** | 57.29% | 70.14% |
| Subject 6 | 54.88% | **61.40%** | 53.82% | 60.76% |
| Subject 7 | 88.80% | 87.36% | 91.67% | **96.53%** |
| Subject 8 | 76.75% | **83.76%** | 81.25% | 81.6% |
| Subject 9 | 74.24% | 78.03% | 79.17% | **83.68%** |
| Mean | 72.39% | 77.34% | 74.30% | **80.32%** |

with an average recognition accuracy improvement of 8%. SRLS-EEGNet also outperformed EEG-TCNet and Shallow ConvNet, models with more advanced structures, thereby affirming the effectiveness of the SRLS method. The classification performance on dataset 2 is displayed in Table 4.

**TABLE 4. Comparison of P300 recognition results.**

| | A01 | A02 | A03 | A04 | A05 | A06 |
|---|---|---|---|---|---|---|
| EEG | 76.9% | 80.1% | 90.2% | 73.0% | 73.3% | 92.4% |
| SRLS | 82.9% | 83.4% | 93.6% | 75.7% | 77.8% | 94.1% |

From the table, it is evident that for the P300 paradigm, SRLS still enhanced the signal recognition accuracy of EEG, with an improvement in performance ranging from 2% to 6%. This advancement could assist researchers in EEG analysis and further corroborates the effectiveness of the SRLS approach.

## IV. DISCUSSION AND CONCLUSION

To conclude, by using the proposed SRLS method, $EEG_{Pl}$ and $EEG_{Dl}$ at different levels can be separated from the original $EEG_T$ according to the correlation $\rho_{ij}$ between the channels and combined as required. The results showed that the proposed method improved the classification accuracies of different types of EEG classification models for most subjects. However, increasing the input data volume in the classification model by Super-resolution greatly increases the need for computing power resources and reduces the speed. Therefore, the proposed method is more suitable for devices with high computing power and low requirement for timeliness or in case the classification accuracy cannot be improved by classification models anymore. If a classification model is designed only for a certain subject, the SRLS method can aid in improving the performance of the model. Moreover, in SRLS, the SR is not restricted to ES-informer. Other models with a good SR effect ought to have a similar effect, which will be verified in future studies.

## REFERENCES

[1] H. Berger, "Über das elektrenkephalogramm des menschen," *Archiv für Psychiatrie und Nervenkrankheiten*, vol. 87, no. 1, pp. 527–570, Dec. 1929, doi: 10.1007/bf01797193.

[2] L. L. Li, G. Z. Cao, H. J. Liang, J. C. Chen, and Y. P. Zhang, "EEG generation of virtual channels using an improved Wasserstein generative adversarial networks," *Lect. Notes Artif.*, vol. 13458, pp. 386–399, Aug. 2022, doi: 10.1007/978-3-031-13841-6_36.

[3] A. Czeszumski, S. Eustergerling, A. Lang, D. Menrath, M. Gerstenberger, S. Schuberth, F. Schreiber, Z. Z. Rendon, and P. König, "Hyperscanning: A valid method to study neural inter-brain underpinnings of social interaction," *Frontiers Human Neurosci.*, vol. 14, p. 39, Feb. 2020, doi: 10.3389/fnhum.2020.00039.

[4] I. Ullah, M. Hussain, E.-U.-H. Qazi, and H. Aboalsamh, "An automated system for epilepsy detection using EEG brain signals based on deep learning approach," *Expert Syst. Appl.*, vol. 107, pp. 61–71, Oct. 2018, doi: 10.1016/j.eswa.2018.04.021.

[5] M. S. Pilato, A. Urban, R. Alkawadri, N. V. Barot, J. F. Castellano, V. Rajasekaran, A. I. Bagióc, and J. S. Fong-Isariyawongse, "EEG findings in coronavirus disease," *J. Clin. Neurophysiol.*, vol. 39, no. 2, pp. 159–165, Feb. 2022, doi: 10.1097/wnp.0000000000000752.

[6] V. Gupta, M. D. Chopda, and R. B. Pachori, "Cross-subject emotion recognition using flexible analytic wavelet transform from EEG signals," *IEEE Sensors J.*, vol. 19, no. 6, pp. 2266–2274, Mar. 2019, doi: 10.1109/JSEN.2018.2883497.

[7] J. R. Wolpaw, N. Birbaumer, W. J. Heetderks, D. J. McFarland, P. H. Peckham, G. Schalk, E. Donchin, L. A. Quatrano, C. J. Robinson, and T. M. Vaughan, "Brain–computer interface technology: A review of the first international meeting," *IEEE Trans. Rehabil. Eng.*, vol. 8, no. 2, pp. 164–173, Jun. 2000, doi: 10.1109/TRE.2000.847807.

[8] R. Na, C. Hu, Y. Sun, S. Wang, S. Zhang, M. Han, W. Yin, J. Zhang, X. Chen, and D. Zheng, "An embedded lightweight SSVEP-BCI electric wheelchair with hybrid stimulator," *Digit. Signal Process.*, vol. 116, Sep. 2021, Art. no. 103101, doi: 10.1016/j.dsp.2021.103101.

[9] S. Liu, D. Zhang, M. Qiao, K. Wang, S. Zhao, Y. Yang, and T. Yan, "Mind controlled vehicle based on LiDAR SLAM navigation and SSVEP technology," presented at the 9th Int. Winter Conf. Brain-Comput. Interface (BCI), Gangwon, South Korea, Feb. 2021.

[10] T. Thenmozhi and R. Helen, "Feature selection using extreme gradient boosting Bayesian optimization to upgrade the classification performance of motor imagery signals for BCI," *J. Neurosci. Methods*, vol. 366, Jan. 2022, Art. no. 109425, doi: 10.1016/j.jneumeth.2021.109425.

[11] O. Attallah, J. Abougharbia, M. Tamazin, and A. A. Nasser, "A BCI system based on motor imagery for assisting people with motor deficiencies in the limbs," *Brain Sci.*, vol. 10, no. 11, p. 864, Nov. 2020, doi: 10.3390/brainsci10110864.

[12] A. Ak, V. Topuz, and I. Midi, "Motor imagery EEG signal classification using image processing technique over GoogLeNet deep learning algorithm for controlling the robot manipulator," *Biomed. Signal Process. Control*, vol. 72, Feb. 2022, Art. no. 103295, doi: 10.1016/j.bspc.2021.103295.

[13] B. Zhang, Z. Zhou, and J. Jiang, "A 36-class bimodal ERP brain–computer interface using location-congruent auditory-tactile stimuli," *Brain Sci.*, vol. 10, no. 8, p. 524, Aug. 2020, doi: 10.3390/brainsci10080524.

[14] G. Xu, Y. Wu, and M. Li, "The study of influence of sound on visual ERP-based brain computer interface," *Sensors*, vol. 20, no. 4, p. 1203, Feb. 2020, doi: 10.3390/s20041203.

[15] J. Choi, K. T. Kim, J. H. Jeong, L. Kim, S. J. Lee, and H. Kim, "Developing a motor imagery-based real-time asynchronous hybrid BCI controller for a lower-limb exoskeleton," *Sensors*, vol. 20, no. 24, p. 7309, Dec. 2020, doi: 10.3390/s20247309.

[16] I. A. Corley and Y. Huang, "Deep EEG super-resolution: Upsampling EEG spatial resolution with generative adversarial networks," presented at the IEEE EMBS Int. Conf. Biomed. Health Informat. (BHI), Vegas, NV, USA, Mar. 2018.
[17] M. Y. Abbass, K.-C. Kwon, M. S. Alam, Y.-L. Piao, K.-Y. Lee, and N. Kim, "Image super resolution based on residual dense CNN and guided filters," *Multimedia Tools Appl.*, vol. 80, no. 4, pp. 5403–5421, Feb. 2021, doi: 10.1007/s11042-020-09824-3.
[18] M. Svantesson, H. Olausson, A. Eklund, and M. Thordstein, "Virtual EEG-electrodes: Convolutional neural networks as a method for upsampling or restoring channels," *J. Neurosci. Methods*, vol. 355, May 2021, Art. no. 109126, doi: 10.1016/j.jneumeth.2021.109126.
[19] Q. She, B. Hu, Z. Luo, T. Nguyen, and Y. Zhang, "A hierarchical semi-supervised extreme learning machine method for EEG recognition," *Med. Biol. Eng. Comput.*, vol. 57, no. 1, pp. 147–157, Jan. 2019, doi: 10.1007/s11517-018-1875-3.
[20] N. Lu, T. Li, X. Ren, and H. Miao, "A deep learning scheme for motor imagery classification based on restricted Boltzmann machines," *IEEE Trans. Neural Syst. Rehabil. Eng.*, vol. 25, no. 6, pp. 566–576, Jun. 2017, doi: 10.1109/TNSRE.2016.2601240.
[21] Z. Khademi, F. Ebrahimi, and H. M. Kordy, "A transfer learning-based CNN and LSTM hybrid deep learning model to classify motor imagery EEG signals," *Comput. Biol. Med.*, vol. 143, Apr. 2022, Art. no. 105288, doi: 10.1016/j.compbiomed.2022.105288.
[22] M. Li, F. Li, J. Pan, D. Zhang, S. Zhao, J. Li, and F. Wang, "The MindGomoku: An online P300 BCI game based on Bayesian deep learning," *Sensors*, vol. 21, no. 5, p. 1613, Feb. 2021, doi: 10.3390/s21051613.
[23] F. R. Willett, D. T. Avansino, L. R. Hochberg, J. M. Henderson, and K. V. Shenoy, "High-performance brain-to-text communication via handwriting," *Nature*, vol. 593, no. 7858, pp. 249–254, May 2021, doi: 10.1038/s41586-021-03506-2.
[24] V. J. Lawhern, A. J. Solon, N. R. Waytowich, S. M. Gordon, C. P. Hung, and B. J. Lance, "EEGNet: A compact convolutional neural network for EEG-based brain–computer interfaces," *J. Neural Eng.*, vol. 15, no. 5, Oct. 2018, Art. no. 056013, doi: 10.1088/1741-2552/aace8c.
[25] X. Deng, B. Zhang, N. Yu, K. Liu, and K. Sun, "Advanced TSGL-EEGNet for motor imagery EEG-based brain–computer interfaces," *IEEE Access*, vol. 9, pp. 25118–25130, 2021, doi: 10.1109/ACCESS.2021.3056088.
[26] A. Craik, Y. He, and J. L. Contreras-Vidal, "Deep learning for electroencephalogram (EEG) classification tasks: A review," *J. Neural Eng.*, vol. 16, no. 3, Jun. 2019, Art. no. 031001, doi: 10.1088/1741-2552/ab0ab5.
[27] S. Zhang, Z. Zhu, B. Zhang, B. Feng, T. Yu, and Z. Li, "The CSP-based new features plus non-convex log sparse feature selection for motor imagery EEG classification," *Sensors*, vol. 20, no. 17, p. 4749, Aug. 2020, doi: 10.3390/s20174749.
[28] A. Jiang, J. Shang, X. Liu, Y. Tang, H. K. Kwan, and Y. Zhu, "Efficient CSP algorithm with spatio-temporal filtering for motor imagery classification," *IEEE Trans. Neural Syst. Rehabil. Eng.*, vol. 28, no. 4, pp. 1006–1016, Apr. 2020, doi: 10.1109/TNSRE.2020.2979464.
[29] G. Placidi, L. Cinque, and M. Polsinelli, "A fast and scalable framework for automated artifact recognition from EEG signals represented in scalp topographies of independent components," *Comput. Biol. Med.*, vol. 132, May 2021, Art. no. 104347, doi: 10.1016/j.compbiomed.2021.104347.
[30] P. Kant, S. H. Laskar, J. Hazarika, and R. Mahamune, "CWT based transfer learning for motor imagery classification for brain computer interfaces," *J. Neurosci. Methods*, vol. 345, Nov. 2020, Art. no. 108886, doi: 10.1016/j.jneumeth.2020.108886.
[31] M. Tangermann, K.-R. Müller, A. Aertsen, N. Birbaumer, C. Braun, C. Brunner, R. Leeb, C. Mehring, K. J. Miller, G. R. Müller-Putz, G. Nolte, G. Pfurtscheller, H. Preissl, G. Schalk, A. Schlögl, C. Vidaurre, S. Waldert, and B. Blankertz, "Review of the BCI competition IV," *Frontiers Neurosci.*, vol. 6, p. 55, Apr. 2012, doi: 10.3389/fnins.2012.00055.
[32] B. Blankertz, G. Dornhege, M. Krauledat, K.-R. Müller, and G. Curio, "The non-invasive Berlin brain–computer interface: Fast acquisition of effective performance in untrained subjects," *NeuroImage*, vol. 37, no. 2, pp. 539–550, Aug. 2007, doi: 10.1016/j.neuroimage.2007.01.051.
[33] K. J. Miller, G. Schalk, E. E. Fetz, M. den Nijs, J. G. Ojemann, and R. P. N. Rao, "Cortical activity during motor execution, motor imagery, and imagery-based online feedback," *Proc. Nat. Acad. Sci. USA*, vol. 107, no. 9, pp. 4430–4435, Mar. 2010, doi: 10.1073/pnas.0913697107.
[34] H. Zhou, S. Zhang, J. Peng, S. Zhang, J. Li, H. Xiong, and W. Zhang, "Informer: Beyond efficient transformer for long sequence time-series forecasting," presented at the AAAI Conf. Artif. Intell., 2021.
[35] T. M. Ingolfsson, M. Hersche, X. Wang, N. Kobayashi, L. Cavigelli, and L. Benini, "EEG-TCNet: An accurate temporal convolutional network for embedded motor-imagery brain–machine interfaces," presented at the IEEE Int. Conf. Syst., Man, Cybern. (SMC), Toronto, ON, Canada, Oct. 2020.
[36] R. T. Schirrmeister, J. T. Springenberg, L. D. J. Fiederer, M. Glasstetter, K. Eggensperger, M. Tangermann, F. Hutter, W. Burgard, and T. Ball, "Deep learning with convolutional neural networks for EEG decoding and visualization," *Human Brain Mapping*, vol. 38, no. 11, pp. 5391–5420, Nov. 2017, doi: 10.1002/hbm.23730.

**HANG SUN** was born in Liaoning, China, in 1994. He is currently pursuing the Ph.D. degree with the Department of Mechanical and Electronic Engineering, Nanjing University of Science and Technology. He is the author of four articles and one inventions. His research interests include computer vision, bioengineering, machine learning, and deep learning. He is also involved in the research of virtual reality and other projects.

**CHANGSHENG LI** received the Ph.D. degree, in 2012. He is currently a Professor with Nanjing University of Science and Technology. He engaged in research in the fields of brain–computer interface, detection guidance and control, and electromagnetic energy storage. He has published multiple SCI and EI articles.

**HE ZHANG** was born in August 1957. He received the Ph.D. degree in measurement technology and instrument from Nanjing University of Aeronautics and Astronautics. He is currently a Professor and a Doctoral Supervisor with the School of Mechanical Engineering, Nanjing University of Science and Technology. He has won two second prize of National Science and Technology Progress, two third prize of Ministry, and enjoys the special allowance of The State Council.